JOURNAL OF ENERGY SYSTEMS

2023, 7(2)

2602-2052 DOI: 10.30521/jes.1160434 Research Article

The heat transfer with nanomaterial enhanced phase change materials in different container shapes

Allan T. Muzhanje*
Egypt Japan University of Science and Technology (E-JUST), Energy Resources Engineering Department, New Borg El-Arab City, Alexandria, Egypt, allan.takudzwa@ejust.edu.eg
Mohsen A. Hassan
Egypt Japan University of Science and Technology (E-JUST), Material Science and Engineering Department, New Borg El-Arab City, Alexandria, Egypt, mohsen.khozami@ejust.edu.eg
Shinichi Ookawara
Tokyo Institute of Technology, Chemical Science and Engineering Department, Tokyo, Japan, sokawara@chemeng.titech.ac.jp
Hamdy Hassan
Egypt Japan University of Science and Technology (E-JUST), Energy Resources Engineering Department, New Borg El-Arab City, Alexandria, Egypt
Assiut University, Assiut, Egypt, hamdyaboali@yahoo.com

Submitted: 08.11.2022
Accepted: 18.03.2023
Published: 30.06.2023

* *Corresponding Author*

Abstract: The heat transfer is studied during the melting and solidification of sp11 and sp24 phase change materials in different container shapes. The materials are further mixed with nano-alumina and nano CuO enhancements. We aim to identify the most favorable phase change material for free-cooling in summer and free-heating in winter. Ansys Fluent 20.2 is used to analyze the 2D models for the melting and solidification mechanisms of the phase change samples in cylindrical, square, rectangular, and elliptical-shaped capsules. The nanomaterial-enhanced phase change material improves the melting and solidification behavior over the base phase change material by as much as 9.8%. It is further observed that the nanomaterial-enhanced phase change material particularly in the rectangular-shaped containers has faster melting and solidification rates by over 43% compared to the others. The material sp24 with 4% nano-alumina in a rectangular profile has the shortest melting times ~70-100 mins, when the inlet temperatures are 313 and 318 K. The same material has the shortest solidification time of 426 mins, two times faster compared to the 928 mins observed with the cylindrical capsule under the same conditions. The Sp11 with the nano-alumina in a rectangular capsule also has a short melting time of 134 mins. The rectangular profile is found capable of achieving the highest temperature drop about 3.3 K during free cooling of inlet air using nano-enhanced sp24. A progress is realized in unmasking the potential of the thermal energy battery using hybrid geometry and nanomaterial enhancements.

Keywords: *Geometry enhancement, Heat transfer, Nano-alumina, Nano-CuO, Phase change material*

Cite this paper as: Muzhanje, A.T, Hassan, M.A, Ookawara, S, & Hassan, H. The heat transfer phenomena of nanomaterial enhanced phase change materials during their melting and solidification cycles in different container-shapes. *Journal of Energy Systems* 2023; *7*(2): 173-186, DOI: 10.30521/jes.1160434

Nomenclature	
$LH\ TES$	Latent Heat Thermal Energy Storage
$NePCM$	Nanomaterial Enhanced Phase Change Material
T	Temperature (K)
H	Enthalpy (J)
k	Thermal Conductivity $(W/m\ K)$
t	Time (s)
p	Momentum $(kg\ m/s)$
u	Velocity (m/s)
g	Acceleration due to gravity $(kg\ m/s^2)$
C_p	Specific Heat Capacity $(J/kg\ K)$
∂	Partial Derivative Operator
μ	Dynamic Viscosity $(Pa\ s)$
β	Liquid Fraction
ρ	Density (kg/m^3)
φ	Nanomaterial Composition $(wt.\%)$

1. INTRODUCTION

The adversity of diminishing natural energy resources against a seemingly insatiable and ever-growing energy-demand drives research efforts towards discovery of more sustainable energy solutions. The global energy consumption grew by almost 6% in 2021 after the economic rebound from the Covid-19 pandemic [1]. Despite the intensification of technologies towards renewables, there remains a mismatch of energy supply against an ever-inflating demand especially due to fluctuating surface temperatures reaching record high levels in several regions around the globe, other factors also include geopolitics, and rising population levels [2]. This consequently pushes up the energy demand particularly for space cooling and heating applications [3]. Reports show that air conditioning has been the fastest growing end-use of energy in buildings for the past four decades [4]. Thermal energy storage (TES) is a presently potent concept amongst sustainable energy studies that can combat the energy crisis [5,6]. Application of TES systems in indoor environment control thereby plays a fundamental role towards energy preservation.

Phase change material (PCM) is used to store and resupply significant amounts of the thermal energy for the future usages, when it is needed [7]. A usefully large amount of energy is absorbed as latent heat of fusion during a phase change i.e., latent heat thermal energy storage (LHTES) [8]. These systems have higher energy storage capacities and they can undergo easily reversible phase change processes [9]. PCM LHTES systems have low maintenance costs, yet capable of achieving significant energy savings in various applications. The material is commercially available e.g., from Rubitherm Technologies GmbH in operating temperature ranges, -50 $^{\circ}$C up to 111 $^{\circ}$C [10], which has allowed several research studies to be contacted on it. Said and Hassan [11], found that use of PCM - LHTES day-to-night temperature changes managed over 7% savings on power usage of an air conditioning system. Literature also recorded that a PCM TES equipped AC system had about 9.1% energy savings and a reduction in CO_2 emissions of around 17% [12]. Another study observed that with enhancement of PCM, there was a 4.1 $^{\circ}$C drop in room temperature and 5% energy savings [7]. Other applications included building envelopes for energy efficient buildings and solar integrated systems which achieved better coefficients of power (COP) >1.0 [13].

PCMs are commonly put in two classes, i.e., the inorganics and organics [14,15]. The organic PCMs are particularly attractive in LHTES in terms of environmental friendliness since they have relatively low toxicity and additionally, minimal supercooling challenges that are much pronounced amongst inorganic PCMs [16]. They, however, have low thermal conductivity and undergo leakage during melting [17]. On the other hand, the inorganic PCMs have higher volumetric energy storage densities, better flame retardancy and slightly improved thermal conductivity [18]. Nanomaterials have proven convenient in improving; the thermal conductivity of PCMs, their phase change performance, retard flammability, and adjust phase change temperatures [19,20]. It was however, observed to affect the latent heat stockpile capacity of the PCM [21]. Several studies cite a reduction in the LH capacity due to the addition of inactive mass [22], whereas other authors note an improvement [23].

Researchers also observed that the optimization of design configuration and dimension had significant effects on the thermal performance of LH TES systems [24]. Some researchers recommended plate configurations from their findings [25], whereas other studies recommended copper pipes [26,27]. The cross section of an elliptical capsule was found to have impact on the melting behavior of PCM whereas the increase in air velocity had negligible effect [28]. An organic RT26 PCM was investigated in circular and elliptical capsules, to show improved heat transfer efficiency by 27%, 49% and 58% for eccentricities, 0.02, 0.04 and 0.06, respectively [29]. Whilst most of the research studies have involved singular geometries comparing PCM types, a few recent works have considered several configurations. One study investigated different shapes of micro-capsules for PCM including a cylinder, hemisphere, cube, frustrum and a sphere [30]. The study concluded that the hemisphere had the best melting rate, and the sphere had the lowest at fixed volume.

Stirred by this background the current study compared the heat transfer process using four macro-sized shapes (i.e., cylindrical, square, rectangular and elliptical geometries), to contain PCM/NePCM in a TES system. For these geometries, the research investigates the melting and solidification behavior with and without 4% nano-alumina and nano copper oxide particles ø45nm for PCM-SP24E for summer and PCM-SP11gel for winter conditions. The PCMs are all supplied by Rubitherm. The SP series PCMs from Rubitherm are inorganic solid liquid-based mixtures of salts, water, and other additives [10].

In the present study, the heat transfer characteristics of the melting and solidification cycles of the four configurations are investigated for PCM with and without nanoparticles. The study is performed for melting at different inlet temperatures 313 K and 318 K for summer, then 293 K for winter in a constant volume. Similarly, solidification is studied for 295 K in summer and 277 K during winter. The analyzed model combinations for the PCMs and NePCMs are aimed at developing a PCM box that will be used for free cooling/heating in a building towards energy savings.

2. MATERIALS AND METHODS

Using the diurnal temperature during a 24 h., day, the PCM or NePCM will melt by absorbing energy from inlet air thereby cooling it to lower indoor temperature. During the night as temperature drops, the cold air at night will carry away the excess energy from the PCM such that it solidifies and becomes ready for another cycle, meanwhile the warm outlet air will be passed indoors to warm the room. The mechanism works similarly in winter where the excess energy from the daily high temperatures will be used to warm the inlet air into the room.

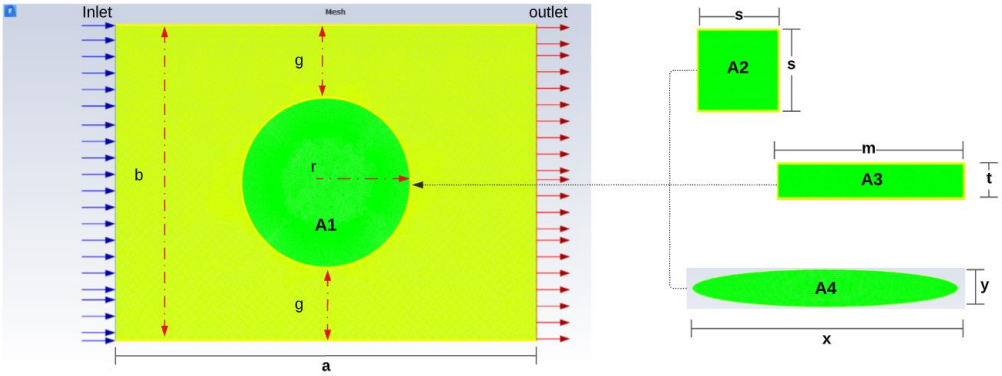

Figure 1. Physical model of the PCM containers of different geometries.

As shown in

Figure 1, molten PCM, which is the base fluid in the study, is considered an incompressible Newtonian fluid of unsteady flow in 2D with constant properties except the density, modeled by the Boussinesq approximation accounting for thermal buoyancy. The NePCM is assumed to be continuous media in thermodynamic equilibrium, with zero velocity slip between solid nanoparticles and the aqueous PCM. The negligible effects of thermal radiation, viscous dissipation and volume expansion are assumed insignificant in the study. Moreover, molten PCM is considered an incompressible, single-phase, and homogeneous fluid also referred to as a nanofluid [31,32].

Table 1. Geometry and mesh details of the system.

Units	cylinder *A1*	square *A2*	rectangle *A3*	ellipse *A4*
mm	*r = 20*	*s = 35.45*	*t = 15*	*y = 15*
			m = 83.78	*x = 106.7*
	a = 100	*a = 106.45*	*a = 150*	*a = 150*

	b = 75	*b = 70.45*	*b =50*	*b = 50*
Mesh elements	*96 126*	*93 727*	*97 278*	*100 542*

2.1. Governing Equations

The liquid/melting fraction, outlet air temperature, and the Nusselt number are obtained from Ansys 20.2 by solving the Navier-Stokes and energy equations coupled to a melting/solidification PCM model. The equations solved include the continuity, momentum and energy equations detailed below [33,34].

Continuity equation is given by,

$$\partial_\tau(\rho) + \partial_i(\rho u_i) = 0. \tag{1}$$

Momentum equation is expressed as follows:

$$\rho\frac{\partial u}{\partial \tau} + \rho\partial_j(u_i u_j) = \mu\partial_{ii}(u_i) - \partial_i(p) + \rho g_i + S_i. \tag{2}$$

Energy equation by the total enthalpy method is given by,

$$\rho\frac{\partial H}{\partial \tau} = \nabla.(k\,\nabla T)\,. \tag{3}$$

Here, S_i is Darcy's source term based on the liquid fraction (β) added to the momentum equation to turn the velocity of liquid cells on and that of solid cells off during the phase transition i.e., in the mushy state. Darcy's source term is expressed as,

$$S_i = \frac{(1-\beta)^2}{\beta^3+\omega} A_{mz}\, u_i, \tag{4}$$

where ω is usually 0.001, a small number ensuring a non-zero divisor and A_{mz} is the mushy zone constant recommended in the orders of $10^3 - 10^8$. The value is 10^5 in this study.

Sensible heat (h_{sn}) is given by,

$$h_{sn} = h_0 + \int C_p dT \tag{5}$$

The enthalpy (H) here becomes,

$$H = h_{sn} + \Delta H \tag{6}$$

ΔH is found in the latent heat term (L) given as:

$$L = \frac{\Delta H}{\beta} \tag{7}$$

where,

$$\beta = \begin{cases} 0 & T < T_s \;\; solid\ state \\ \dfrac{T - T_s}{T_l - T_s} & T_s \le T < T_l \;\; mushy\ zone \\ 1 & T \ge T_l \;\; liquid\ state \end{cases} \tag{8}$$

Thermal and physical properties for PCM [10] and nanomaterial are shown in Table 2 [33]

Table 2. Thermo-physical properties of PCM & nanomaterial [35]

Materials		sp11	sp24	Al_2O_3	CuO
Density	kg/m^3	1330	1500	3600	6320
C_p	J/kg K	2000	2000	765	535.6
k	W/m K	0.6	0.5	36	40
μ	mm^2/s	111.1	111.1	----	----
α	1/K	0.001	0.001	----	----
Latent heat	kJ/kg	155	180	----	----

The properties of the nano-enhanced phase change material (NePCM) are solved using the following Eqs. [9-14] where subscripts *c*, *n* and *sp* denote the composite-PCMs', the nanoparticles' and the PCM properties, respectively [36]. The effective density of the NePCM composite is,

$$\rho_c = \varphi\rho_n + (1 - \varphi)\,\rho_{sp}. \tag{9}$$

The specific heat capacity,

$$C_{p_c} = \frac{\varphi\rho_n C_{p_n} + (1 - \varphi)\,\rho_{sp} C_{p_{sp}}}{\rho_c}, \tag{10}$$

The effective dynamic viscosity (μ),

$$\mu_c = A_1 e^{(A_2 \cdot \varphi)}(\mu_{sp}), \tag{11}$$

The thermal conductivity,

$$k_c = \frac{k_n + 2k_{sp} - 2(k_{sp} - k_n)\,\varphi}{k_n + 2k_{sp} - (k_{sp} - k_n)\varphi} k_{sp} + 5\,(10^4)\,(\gamma)(\varphi)(\rho_{sp})\left(C_{p_{sp}}\right)\sqrt{\frac{B_z\ T}{\rho_n\,\emptyset_n}}(f(T,\varphi)) \tag{12}$$

$f(T,\varphi)$ is usually taken as,

$$f(T,\varphi) = [2.8217\,(10^{-2})\,\varphi + 3.917\,(10^{-3})]\left(\frac{T}{T_o}\right) + [-3.0669\,(10^{-2})\,\varphi\ - 3.91123\,(10^{-3})], \tag{12b}$$

where γ is given in Table 3, B_z is Boltzmann's constant 1.381 (10^{-23}) J/K., T_o is reference temperature. The latent heat is,

$$L_c = \frac{(1 - \varphi)\,(\rho_{sp}.L_{sp})}{\rho_c} \tag{13}$$

Thermal expansion coefficient (α_c) is given below following Ref. [37],

$$\alpha_c = \frac{(1-\varphi)\,(\rho_{sp}.\alpha_{sp}) + \varphi\,(\rho_n.\alpha_n)}{\rho_c}. \tag{14}$$

Table 3. Curve-Fit Coefficients [38], for Eqs. (10-12)

	A	A_1	A_2	*B*	γ	*C*	φ [%]	*T* [K]
Al_2O_3	0.000891	0.9830	12.959	0.5179	$8.44(100\,\varphi)^{-1.073}$	0.425	$1.0 \le \varphi \le 10$	$298 \le T \le 363$
CuO	--	0.9197	22.854	--	$9.88(100\,\varphi)^{-0.9446}$	--	$1.0 \le \varphi \le 10$	$298 \le T \le 363$

2.2. Initial and Boundary Conditions

The PCM is a static solid, inlet air is at constant velocity and temperature at τ = (0 s). At boundaries, there is no slip, no reverse flow, gauge pressure is 0 Pa, and the walls are adiabatic. A pressure based fluent solver in single precision is used with velocity formulation of the 2D transient model. The energy, solidification/melting, and the k-€, 2^{nd} order realizable viscosity models are used. The solution scheme is SIMPLE pressure velocity coupling with a PRESTO pressure scheme. Energy, momentum, and dissipation rates are set to 2^{nd} order upwind and the transient formulation to first order implicit functions. The relaxation factors are 0.3, 1, 0.7, 0.9 and 1 are used for pressure, density, momentum, liquid fraction, and energy respectively.

2.3. Validation of the Model

For a small constant cross-sectional area $0.00126\ m^2$ and equal volume, the time step of 1 s and the mesh elements in Table 1 are found sufficient. Figure 2(a,b) shows the time-step and mesh independency establishments, respectively. The model used here was experimental validated for PCM plates [11] as shown in Fig. 2(c). From Figure 2(c), the highest error between numerical and experimental results was about 4% for the studied cases.

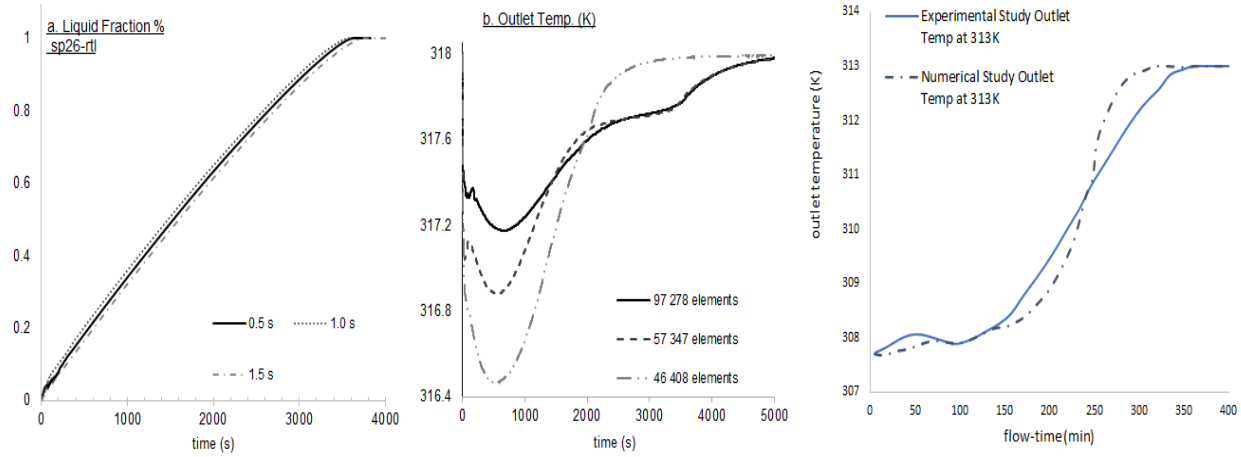

(a) *(b)* *(c)*

Figure 2. (a)Time step, (b)mesh dependency and (c)validation of model.

3. RESULTS AND DISCUSSION

The results presented here show the heat transfer phenomena of winter based PCM sp11 and the summer based sp24, with and without nanomaterial addition. The respective nano-enhanced composites are labeled nalsp11, ncuosp11 and nalsp24, ncuosp24, respectively. The containers are indicated for each line on the graphs as *C*, *S*, *R* and *E*, for cylinder, square, rectangle, and ellipse, respectively. The reported results show the effect of the *(i)* geometric enhancements from the cylindrical shape to the other three profiles and *(ii)* nanomaterial addition to the melting performance of the PCMs.

Using a circular model as the datum, the heat transfer increases towards the thin profiles in the order, circular, square, elliptical and rectangular. The nanomaterial addition enhances the heat transfer due to the conductive material being added to the PCM to function as heat conductor particles. Alumina nanomaterial has the best performance against nano CuO. The study discusses, the rates, the outlet temperature profiles, the capsule surface heat flux and the heat transfer coefficient of the contact region as these are indicative of the performance of the TES device.

3.1. Effect of the Enhancements on the Melting Rate

Figure 3(a-c), show the melting fractions of sp11 at 293 K, sp24 at 313 and sp24 at 318 K, respectively. The rectangular profile has the most improved melting rates taking the least melting time in all cases. Nano-alumina

enhanced - sp11 in a rectangular capsule has the fastest melting rate of 134 mins, compared to the other combinations.

3.1.1 Effect of the geometry enhancement

In the order *C, S, E, R*, the complete melting times before nanomaterial addition for sp11 were 253, 207, 158 and 143 mins, respectively at 293 K (Figure 3(a)). This reflects a 43.48% improvement of the rectangular profile from the cylindrical, 37.55% for ellipse and 18.18% improvement for the square profile. It is expected that the effect can be slightly higher at higher outlet temperatures. This can be attributed to the increased active heat transfer surface, which is found in flattened geometries over wide blunt or large curved faces such as those of the square and circular cylinders. The thin blunt edge of the rectangular cylinder has advantage of slightly retaining air molecules on the incident face of the capsule without creating large wakes that can break the airflow contact with the rest of the capsule. Wider blunt geometries however, have bigger areas of eddies and no contact on the capsule surface boundary because of high resistance to flow, which reduces the effectiveness of heat transfer. This similar behavior is recorded in the case of sp24. At 313 K, the complete melting time of sp24 in the circular, square, elliptical and rectangular capsules is 96, 106, 147 and 176 mins, respectively. The heat transfer enhancement of 45.45%, 39.77%, and 16.48% are realized in the rectangular, elliptical, and square profiles respectively. The rate is faster at higher inlet temperatures as can be witnessed at 318 K, where it takes 74, 82, 114 and 138 mins to melt sp24 in *R, E, S* and *C* profiles, respectively. The percentage enhancements are like the other discussed cases at this temperature, following the same mechanisms of heat transfer described before.

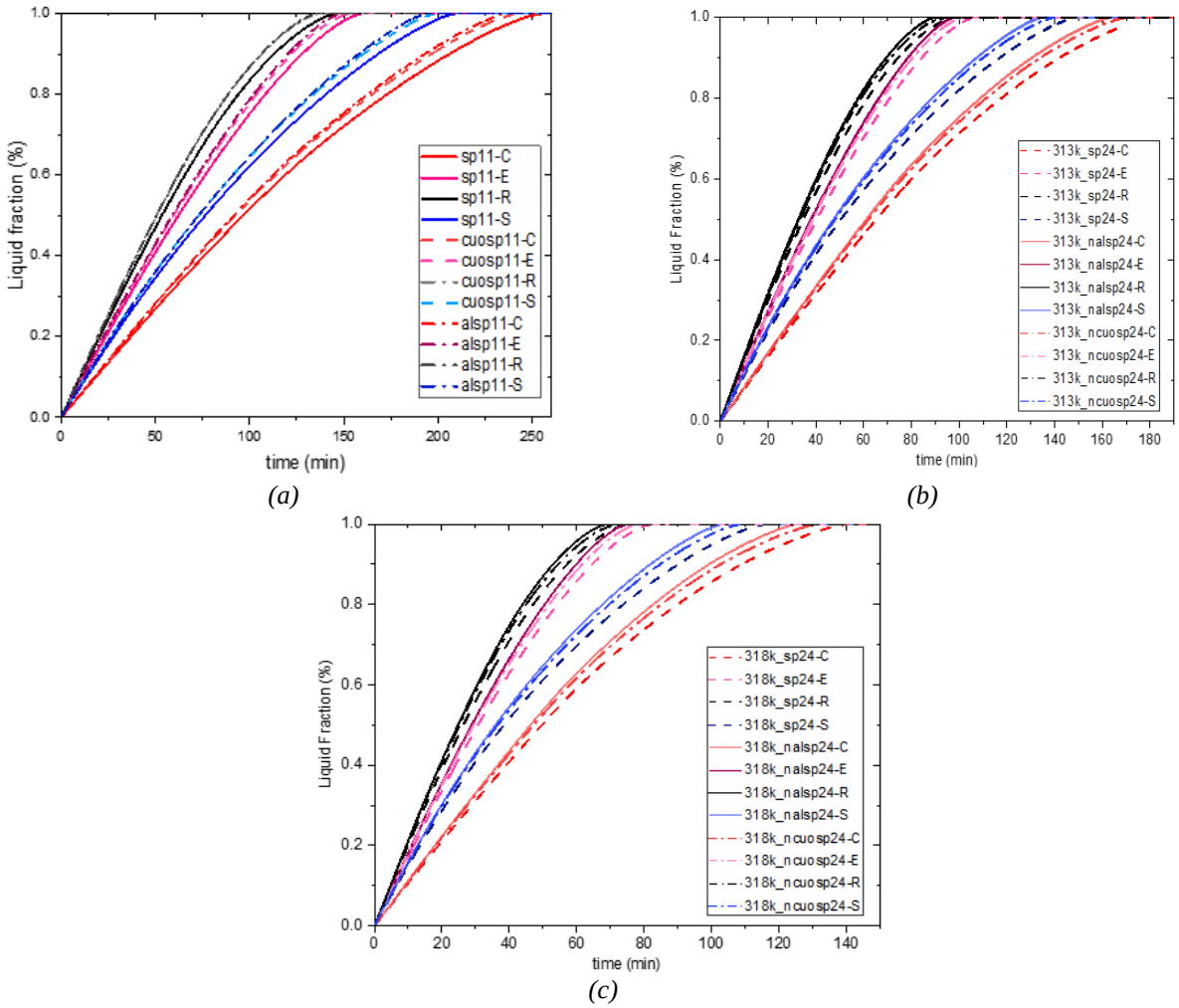

Figure 3. Liquid fraction graphs (a) Sp11 at 293 K (b) Sp24 at 313 K & (c) Sp24 at 318 K

3.1.2 Effect of the nanomaterial addition

The melting times also reduce with the addition of nanomaterial additives, and the phenomena is pronounced with nano-alumina particles which gives, 134, 146, 192 and 235 mins for sp11 in *R, E, S* and *C* shape profiles, respectively. The percentage enhancement due to this nanomaterial therefore approximates 6.49%, 7.59%, 7.25% and 7.51% for the respective profiles. Addition of nano CuO yielded, 4.90%, 5.06%, 5.31% and 5.14% enhancements in the same respective shapes. This is because of the densities of the nanoparticles. Even though nano CuO particles have higher thermal conductivity 40 $W/m\,K$ > 36 $/m\,K$, they also weigh (6320 kg/m^3) almost twice as the nano-alumina (3600 kg/m^3) particles such that for the same composition, the nano-alumina particles are likely to vibrate and move faster within the nanofluid when subjected to a packet of energy compared to the CuO.

With the sp24, it similarly follows that nano-alumina particles have 7.61, 8.40, 9.07 and 8.12% thermal enhancement in the *R, E, S* and *C* profiles respectively at 313 K. At higher thermal gradients, the melting rate further increases and the percentage enhancements by the nanomaterial addition become 7.99, 9.72, 9.83 and 9.16% in the respective shapes presented in the latter scenario. With this PCM, the effect of the nano CuO is also observed to be lesser than that of nano-alumina at 4.55%, 5.44%, 5.46% and 5.66% for *R, E, S* and *C* profiles respectively. It is noted that the percentage enhancement is slightly lower in the rectangular profile and relatively comparable in the other profiles. This is attributed to the promotion of convection heat transfer which is better within the other profiles compared to the rectangular profile.

3.2. Effect of the Enhancements on the Solidification Rate

Solidification follows the same heat transfer behavior as the melting process only that this time, conductivity reduces with time as opposed to melting. Because the PCM agglomerates, there is increased inertia on the nanomaterial vibrations and movements, reduced convection, and thermal conductivity such that it can be concluded that the heat transfer rate reduces with time. The solidification process takes longer than the melting, 426, 469, 607 and 928 mins for nano-alumina enhanced - sp24 to completely solidify at 295 K in the *R, E, S,* and *C* capsules. For the sp11 it takes 120, 131, 173 and 212 mins for the respective geometries. Similar behavior is noted for the nano enhancements with monotonic trends as previously described during the melting. Percentage improvement due to the alumina nanomaterial is 6.98, 9.03, 7.9 and 7.8% in the *R, E, S* and *C* profiles respectively. Nano - CuO enhancements average 4.97%.

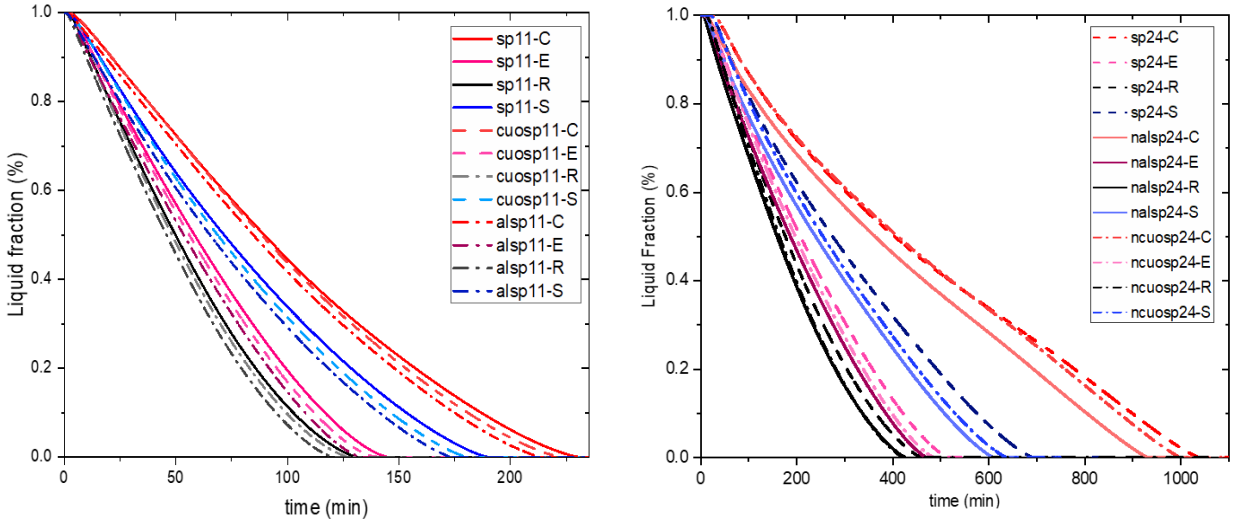

(a) *(b)*

Figure 4. Solidifcation graphs: (a) sp11 at 277 K, (b)sp24 at 295 K

3.3. Response of the Outlet Temperatures to the Enhancements

Outlet temperature profiles were investigated under the different conditions for both sp11 and sp24 during melting and solidification cycles. The data in Figs. 5(a-c) showed the air cooling and heating effects of the PCM device. During the melting process, the temperature rapidly drops withing the first 0 – 2 mins, sharply

gains for a few seconds then steadily increases until the end of the melting process when the temperature reaches equilibrium i.e., 293 K for sp11, 313 or 318 K for sp24.

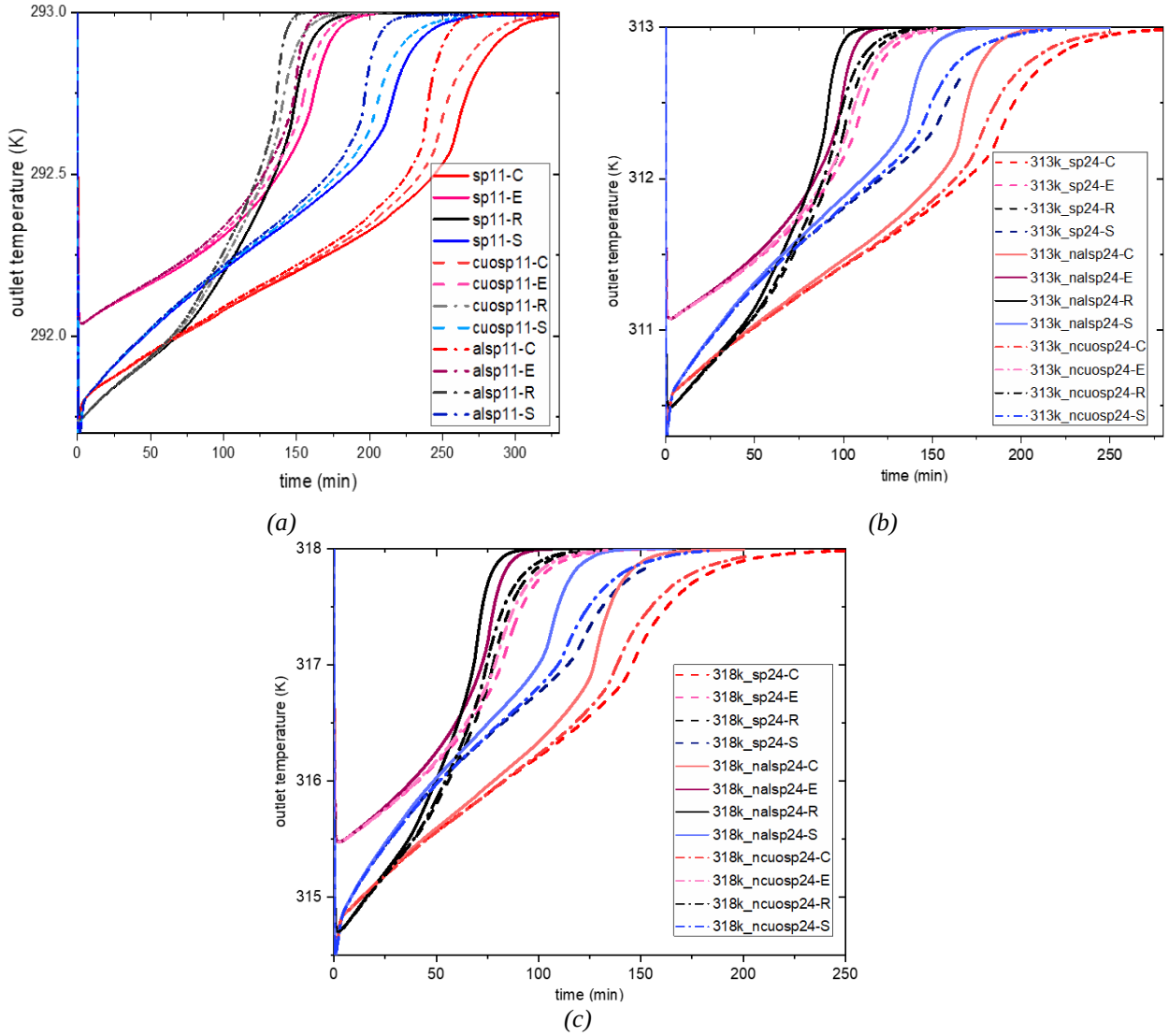

Figure 5. Outlet temperature graphs: (a) sp11 at 293 K, (b) sp24 at 313 K, and (c) sp24 at 318 K.

3.3.1 Outlet temperature during melting cycles

The outlet temperature describes the degree of free cooling/heating of the capsule, when a stream of inlet air blows over the capsule surface in the TES heat exchanger unit. The PCM starts from cold as a stationary solid which absorbs thermal energy from ambient air inlet to the TES during the melting stage. Initial sharp drop is due to the sudden stop of air molecules at the edges of the capsule incident to the incoming stream. The system however, quickly stabilizes and the flow adopts a steady incline during which period the thermal energy in hot air particles/molecules is absorbed, the air molecules are cooled and passed out at a lower temperature, until the system is fully charged with heat energy, i.e., completely molten. During this process, the rectangular profile can be seen to have lowest outlet temperatures for all cases meaning better cooling potential. With sp11 at 293 K, the profiles, *E, C, S,* and *R* can manage reduction of inflow-air temperature by 1.0, 1.21, 1.21 and 1.3 K (see in Figure 5(a)). For the material Sp11, it is more desirable for the material to have more free-heating potential during the solidification process, as this will be its main function during winter seasons.

Figure 5(b) shows the degree of cooling of the sp24 at 313 K, where the degree of cooling is 1.93 K for the ellipse, 2.41 K apiece for cylinder and square then 2.51 K for the rectangular capsule, which is the largest. Due to enhanced heat transfer characteristics in the rectangular profiles, better cooling potential is observed herein.

This potential is more pronounced with higher thermal gradients as presented in Figure 5(c) for inlet temperature 318 K showing that the capsules in order of ascending performance. Strictly speaking, *E*, *C*, *S* and *R* can achieve 2.53, 3.15, 3.15 and 3.3 K temperature drops, respectively. The best performances in this regard for sp24 are most desired during this melting process as the material is dedicated to offer free cooling during a hot day, by drawing hot ambient air and absorbing its thermal energy to offer a cooler indoor atmosphere.

Nanomaterial samples only improve the rate of change of the temperature in the order discussed in the previous section, but they do not affect the magnitude of the temperature drop. It therefore proofs that cooling can be achieved quickly by using the rectangular capsules. In the case of multiple capsules, the degree of cooling can be magnified by the number of capsules for realization of higher benefits.

3.3.2 Outlet temperature during solidification

During the solidification process, the inlet air mass is cooler than the PCM, which is completely molten such that the temperature gradient favors transfer of heat energy to the cold air molecules from the PCM capsule i.e., from the PCM. The greater the thermal gradient between the air molecule and the contact region of the capsule, the more the heat that will be absorbed from the PCM.

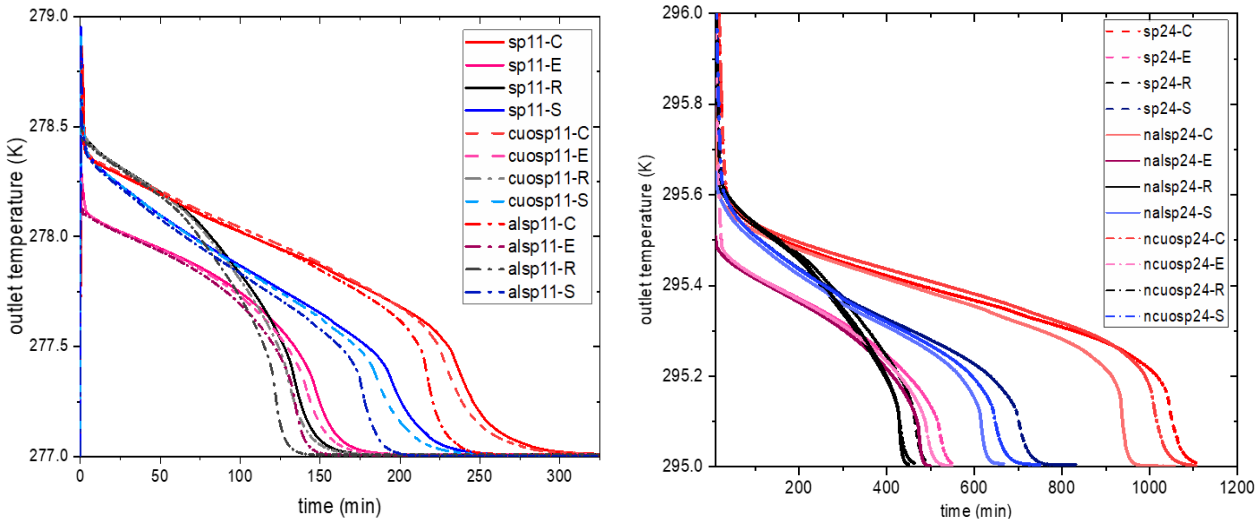

(a) *(b)*

Figure 6. The outlet temperature graphs: (a) on the left sp11 at 277 K, (b) on the right sp24 at 295 K.

When air mass at 277 K was constantly blown over the geometries with sp11 at 289 K, it was observed that the inlet air was heated until the temperature of the PCM is uniformly at 277 K. Here, the PCM would have solidified as shown in Figure 6(a). The temperature was sharply increased as air started sweeping over the hot surface then steadily dropped until complete solidification at the point, where it reached at the equilibrium temperature. It was observed that during this process, the outlet temperature using sp11 increases by 1.46, 1.11, and 1.35 K for capsules *R*, *E*, *C* and *S*, where *C* and *S* have the same value. Similarly, in the sp24 scenario, the temperature increase reached up to 0.62 K for the rectangular profile. This would have supplied additional heating if a hybrid material mixed with sp11 and sp24 for free heating and cooling applications was to be considered.

3.4. The Heat Transfer Coefficient on the Contact Region

Since the heat transfer coefficient measures the rate of heat transfer from the solid thermal boundary to the heat transfer fluid, this study presents the heat transfer for four shapes by using sp11 at 277 K and sp24 at 318 K, because the trend is monotonic for all cases with slight differences with temperature.

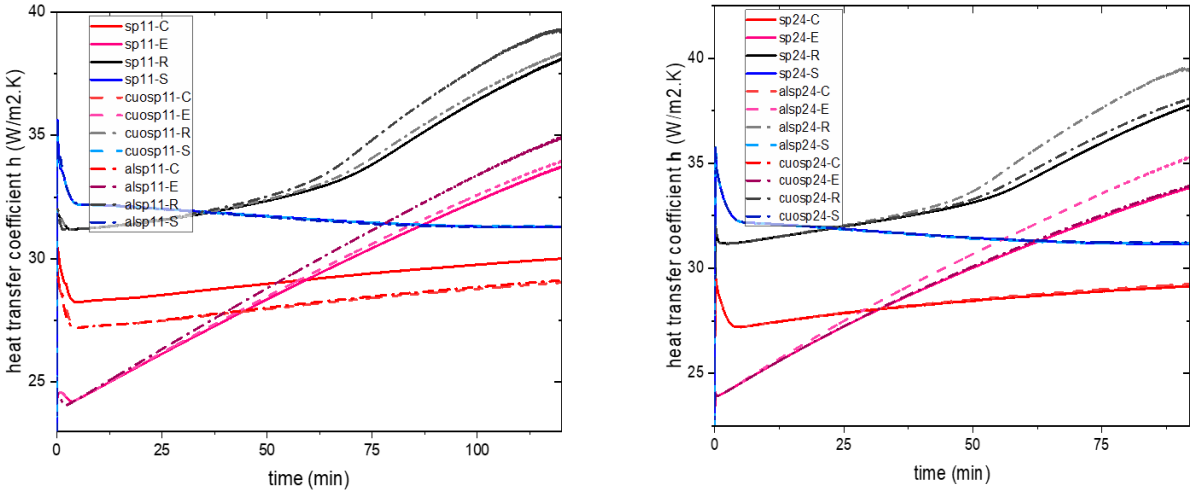

(a) *(b)*

Figure 7. Heat transfer coefficient graphs: (a) sp11 at 277 K, (b) sp24 at 318 K.

The rate of heat transfer is seen to perform the best in the rectangular profile at heat transfer coefficient 37 – 40 $W/m^2\ K$, this is due to the availability of a larger active heat transfer surface as indicated earlier, which improved the heat flux of the surface. Moreover, addition of the nanomaterial supporting the heat transport within the PCM also enhanced the coefficient as could be seen in Figure 7(a,b). The ellipse had the second highest *h* coefficient as witnessed from its fast- melting rates presented earlier, arising from the discussed heat transfer mechanism in flattened geometries. The effect of nanomaterial enhancement was also witnessed such that, the coefficients were 33 and 35 $W/m^2\ K$, for the elliptical profile increasing with nano-CuO and nano-alumina respectively. The square profile had a range of 31 – 32 $W/m^2\ K$ and the cylinder had 29 – 30 $W/m^2\ K$. This was witnessed in all the studied cases and the range did not deviate much with different scenarios, e.g., *h* for sp11-*S* at 277 K is 31.11 $W/m^2\ K$, whereas for Sp24-*R* at 318 K it is 31.37 $W/m^2\ K$. Similar results were obtained at 313 K with sp24 and at 293 K with sp11 and their composites. It can be concluded that the heat transfer coefficient was the highest for the rectangular profile, and for flat geometries. Furthermore, it was improved by the use of nanomaterial especially lightweight, high thermal conductivity nanomaterials.

3.5. Capsule Wall Heat Flux

The flux density over the capsule described the amount of heat transferred to the inlet air per square meter of the surface. The general patterns of this behavior were briefly illustrated for the sp11 and compared for sp24 at 313 K and 318 K before the usages of nanomaterials. The magnitude of the thermal flux over the contact region proofed that heat was exchanged via the heat transfer fluid. During the melting process, because heat was extracted from the environment (in this case, inlet air) and added into the PCM, thereby heat flux was negative and vice versa for the solidification process. In the present study, during the melting of sp24, the heat flux rapidly dropped to below minus 700 W/m^2, raised sharply followed by a steady incline until completion of phase change process, then it became a flat line in Figure 8(a,b). The heat flux reached the lowest troughs, and maximum peaks in the rectangular and square profiles e.g., ~ 300 W/m^2 for sp11 at 277 K (Figure 8(a,b)). The ellipse had the smallest magnitudes ~ 200 W/m^2 for sp11 at 277 K and ~ - 375 W/m^2 for sp24 at 313 K Figure 8(a). As expected, the heat flux was increased by the inlet temperature. Figure 8(a) shows that nanomaterial addition does not have an influence on the magnitude of the heat flux, however, it increases the rate of change of the heat flux in the similar fashion.

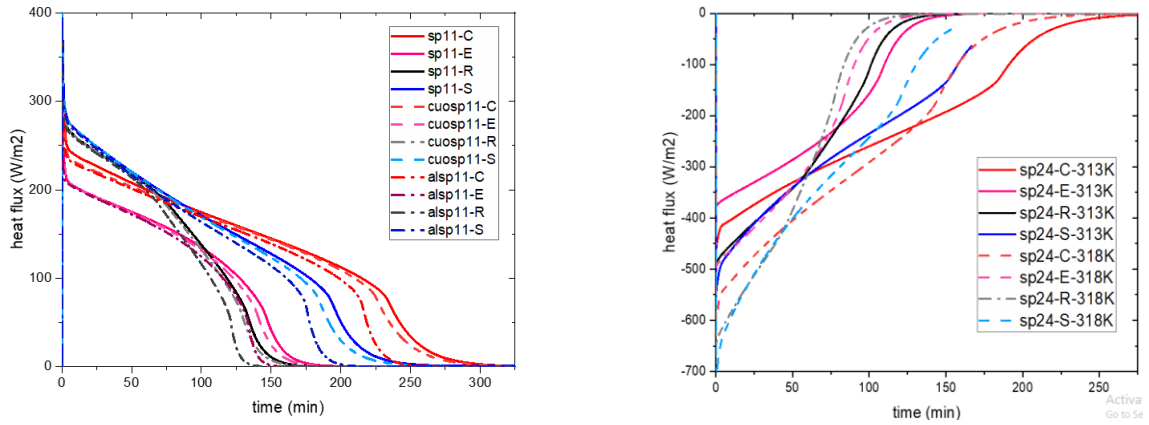

(a) *(b)*

Figure 8. Heat flux plots for sp11 and sp24 at the contact regions.

The variation of the heat flux is determined by the temperature gradients incident in the surface as well as the thermal coefficient of the surface. These two factors discussed in the latter sections can be attributed to the behavior of the heat flux, where the rectangular profile has the highest thermal coefficients and reasonable temperature gradients thus it also has the highest heat flux. Similarly matching the coefficients to temperature gradients of the rest of the profiles, the trends illustrated in the Figure 8(a,b), can be traced.

4. CONCLUSION

An investigation of the effect of geometry enhancement and nanomaterial addition on a phase change material-capsule for thermal energy storage was performed numerically using Ansys Fluent 20.2. The study focused on two phase change materials sp11, operating well under winter conditions and sp24, operating well under summer conditions. The material was modeled in 2D simple shaped models, the rectangle, square, ellipse, and circular profiles, 4.0 wt.% nanomaterial was then added to the models to simulate nano enhanced phase change composites, whose heat transfer behavior gave instrumental results. Use of the rectangular capsule over use of the circular profile combined with the addition of 4.0% alumina-nanomaterials to the base PCM, boosted the melting and solidification rates of the PCM-TES model. It also achieved the highest degree of free heating and free cooling. Therefore, rectangular geometries combined with nanomaterial enhancement be considered for a more potent sp11/sp24 phase change material thermal energy system design for winter/summer conditions. The rectangular profile had the highest melting and solidification rate improvement with 43 – 45%. The sp24 was found to have shortest melting time of 70 – 100 mins in the rectangular geometry with alumina-nanomaterial enhancements being the best performing of the studied cases. The percentage nanomaterial driven melting rate enhancements for nano-alumina were concluded to be at least 7.6% with sp24, whereas CuO had from ~ 4.5 – 6.1% improvement. For the solidification process, the rectangular profile with alumina-nanomaterial was the best performing at 426 mins compared to the 928 mins needed in the cylindrical geometry of under the same conditions. For Sp11, a minimum of 230 - 253 mins were needed for complete melting in the circular profile. With the enhancements, these melting times were reduced to 134-143 minutes using the rectangular geometry and 4.0% nanomaterial enhancement.

It was concluded that a drop in temperature of 3.3 K could be realized from using a rectangular profile with alumina-nanomaterial enhanced-Sp24. The material sp11 was found to manage a maximum temperature increase of 1.46 K with the enhancements. It was recorded that the magnitudes of heat transfer coefficient, the outlet temperature and the heat flux were not disturbed by the addition of nanomaterial, but it increased the rate of change of heat transfer with time. The most preferred geometry, the rectangular, was observed to have an h coefficient of 37 – 40 $W/m^2\ K$ and heat flux magnitudes beyond -700 W/m^2. Not only did the study discover evidence of heat transfer improvement with nanomaterial addition, but also found that when the combination of geometry enhancements was used together with highly conductive lightweight nanomaterial,

the melting/solidification rate performance of a phase change material based thermal energy storage device could be improved by nearly 50%.

Acknowledgment

Gratitude is extended to the University and all the Sponsors of the research efforts: EJUST, TCAD-7 partners for the scholarship of the researcher, and the Science, Technology & Innovation Funding (STDF) agency which is sponsoring the research work under the Call 08 of the STDF Project No. 43566 to conduct this study.

REFERENCES

[1] BP, BP Statistical Review of World Energy globally consistent data on world energy markets., 2022. https://www.bp.com/content/dam/bp/business-sites/en/global/corporate/pdfs/energy-economics/statistical-review/bp-stats-review-2022-full-report.pdf.

[2] Turner, J, Lu, H, King, J, Marshall, G.J, Phillips T, Bannister, D, Colwell, S. Extreme temperatures in the Antarctic. *Journal of Climate* 2021; *34*: 2653–2668. DOI: 10.1175/JCLI-D-20-0538.1.

[3] IEA, IEA 2020, Cooling Report, IEA, Paris, 2020. https://www.iea.org/reports/cooling.

[4] IEA, IEA 2019, News: space cooling, IEA. 2019; 1. https://www.iea.org/news/air-conditioning-use-emerges-as-one-of-the-key-drivers-of-global-electricity-demand-growth,13 April 2021.

[5] Selvnes, H, Allouche, Y, Manescu, R.I, Hafner, A. Review on cold thermal energy storage applied to refrigeration systems using phase change materials. *Thermal Science and Engineering Progress* 2021; *22*: 100807. DOI: 10.1016/j.tsep.2020.100807.

[6] Gad, R, Mahmoud, H, Ookawara, S, Hassan,H. Energy, exergy, and economic assessment of thermal regulation of PV panel using hybrid heat pipe-phase change material cooling system. *Journal of Cleaner Production* 2022; *364*: 132489. DOI: 10.1016/J.JCLEPRO.2022.132489.

[7] Rathore, P.K.S, Shukla, S.K. Enhanced thermophysical properties of organic PCM through shape stabilization for thermal energy storage in buildings: A state of the art review. *Energy and Buildings* 2021; *236*: 110799. DOI: 10.1016/j.enbuild.2021.110799.

[8] Li, C, Zhang, P, Li, Q, Tong, L, Wang, L, Ding, Y. Latent Heat Storage Devices, in: Y. Ding (Ed.). *Thermal Energy Storage: Materials, Devices, Systems and Application* 2021; 265–328. DOI: 10.1039/9781788019842-00265.

[9] Riahi, S, Jovet, Y, Saman, W.Y, Belusko, M, Bruno, F. Sensible and latent heat energy storage systems for concentrated solar power plants, exergy efficiency comparison. *Solar Energy* 2021; *180*: 104–115. DOI: 10.1016/J.SOLENER.2018.12.072.

[10] Rubitherm Technologies GmbH, Rubitherm Phase Change Material, Https://Www.Rubitherm.Eu/Index.Php/Produktkategorie/Anorganische-Pcm-Sp. 2021.

[11] Said, M.A, Hassan, H. Parametric study on the effect of using cold thermal storage energy of phase change material on the performance of air-conditioning unit. *Applied Energy* 2018; *230*: 1380–1402. DOI: 10.1016/j.apenergy.2018.09.048.

[12] Omara, A.A.M, Abuelnour, A.A.A. Improving the performance of air conditioning systems by using phase change materials: A review. *International Journal of Energy Research* 2019; *43*: 5175–5198. DOI: 10.1002/er.4507.

[13] Gao, D.C, Sun, Y.J, Ma, Z, Ren, H. A review on integration and design of desiccant air-conditioning systems for overall performance improvements. *Renewable and Sustainable Energy Reviews* 2021; *141*: 110809. DOI: 10.1016/j.rser.2021.110809.

[14] Muzhanje, A.T, Hassan, M.A, Ookawara, S, Hassan, H. An overview of the preparation and characteristics of phase change materials with nanomaterials. *Journal of Energy Storage* 2022; *51*: 104353. DOI: 10.1016/J.EST.2022.104353.

[15] Muzhanje, A.T, Hassan, M.A, Hassan, H. Phase change material based thermal energy storage applications for air conditioning: Review. *Applied Thermal Engineering* 2022; *214*: 118832. DOI: 10.1016/j.applthermaleng.2022.118832.

[16] Leong, K.Y, Abdul Rahman, M.R, Gurunathan, B.A. Nano-enhanced phase change materials: A review of thermo-physical properties, applications and challenges. *Journal of Energy Storage* 2019; *21*: 18–31. DOI: 10.1016/j.est.2018.11.008.

[17] Zhang, G, Yu, Z, Cui, G, Dou, B, Lu, W, Yan, X. Fabrication of a novel nano phase change material emulsion with low supercooling and enhanced thermal conductivity. *Renewable Energy* 2020; *151*: 542–550. DOI: 10.1016/j.renene.2019.11.044.

[18] Lin, Y, Cong, R, Chen, Y, Fang, G. Thermal properties and characterization of palmitic acid/nano silicon dioxide/graphene nanoplatelet for thermal energy storage. *International Journal of Energy Research* 2020; *44*:

5621–5633. DOI: 10.1002/er.5311.
[19] Du, X, Qiu, J, Deng, S, Du, Z, Cheng, X, Wang, H. Flame-retardant and solid-solid phase change composites based on dopamine-decorated BP nanosheets/Polyurethane for efficient solar-to-thermal energy storage. *Renewable Energy* 2021; *164*: 1–10. DOI: 10.1016/J.RENENE.2020.09.067.
[20] Mazur, N, Huinink, H, Fischer, H, Donkers, P, Adan, O. Impact of CsF on phase transitions of K2CO3, In: ECRES 2022 10. European Conference on Renewable Energy Systems; 07-09 May 2022: Istanbul, Turkey, pp. 11.
[21] Yadav, A, Barman, B, Kumar, V, Kardam, A, Shankara, S.N, Verma, A, Madhwal, D, Shukla, P, Jain, V.K. A Review on Thermophysical Properties of Nanoparticle-Enhanced Phase Change Materials for Thermal Energy Storage. *Recent Trends in Materials and Devices* 2017: *178*; 37–47. DOI: 10.1007/978-3-319-29096-6_5.
[22] Luo, Z, Zhang H, Gao X, Xu T, Fang Y, Zhang Z. Fabrication and characterization of form-stable capric-palmitic-stearic acid ternary eutectic mixture/nano-SiO2 composite phase change material. *Energy and Buildings* 2017; *147*: 41–46. DOI: 10.1016/j.enbuild.2017.04.005.
[23] Döğüşcü, D.K, Hekimoğlu, G., Sarı A. High internal phase emulsion templated-polystyrene/carbon nano fiber/hexadecanol composites phase change materials for thermal management applications. *Journal of Energy Storage 2021*; 39. DOI: 10.1016/j.est.2021.102674.
[24] Ručevskis, S, Akishin, P, Korjakins, A. Parametric analysis and design optimisation of PCM thermal energy storage system for space cooling of buildings. *Energy and Buildings* 2020; *224*. DOI: 10.1016/j.enbuild.2020.110288.
[25] Said, M.A, Hassan, H. Impact of energy storage of new hybrid system of phase change materials combined with air-conditioner on its heating and cooling performance. *Journal of Energy Storage* 2021; *36*. DOI: 10.1016/j.est.2021.102400.
[26] Chaiyat, N. Energy and economic analysis of a building air-conditioner with a phase change material (PCM). *Energy Conversion and Management* 2015; *94*: 150–158. DOI: 10.1016/j.enconman.2015.01.068.
[27] Hassan, H, Harmand, S. Effect of using nanofluids on the performance of rotating heat pipe. A*pplied Mathematical Modelling* 2015; *39*: 4445–4462. DOI: 10.1016/j.apm.2014.12.023.
[28] Sultan, M, Mostafa, H, El boz, A, Elngiry, E. Effect of Inlet and Geometrical Parameters on the Melting of PCM Capsules of Elliptical Cross Section. *ERJ. Engineering Research Journal*. 2021; *44*: 11–20. DOI: 10.21608/erjm.2021.42713.1041.
[29] Alaraji, A, Alhussein, H, Asadi, Z, Ganji, D.D. Investigation of heat energy storage of RT26 organic materials in circular and elliptical heat exchangers in melting and solidification process. *Case Studies in Thermal Engineering* 2021; *28:* 101432. DOI: 10.1016/j.csite.2021.101432.
[30] Sharma, A, Dewangan, S.K. Performance analysis of melting behavior of phase change material encapsulated within differently shaped macro-capsule. *International Journal of Energy and Environmental Engineering* 2022; *13*: 377–394. DOI: 10.1007/s40095-021-00431-y.
[31] Chiam, H.W, Azmi, W.H, Adam, N.M, Ariffin, M.K.A.M. Numerical study of nanofluid heat transfer for different tube geometries – A comprehensive review on performance. *International Communications in Heat and Mass Transfer* 2017; *86*: 60–70. https://doi.org/10.1016/J.ICHEATMASSTRANSFER.2017.05.019.
[32] Hassan, H, Harmand, S. 3D transient model of vapour chamber: Effect of nanofluids on its performance. *Applied Thermal Engineering* 2013; *51*: 1191–1201. DOI: 10.1016/j.applthermaleng.2012.10.047.
[33] Said, M.A, Hassan, H. A study on the thermal energy storage of different phase change materials incorporated with the condenser of air-conditioning unit and their effect on the unit performance. *Energy and Buildings* 2019; *202*: 109353. DOI: 10.1016/j.enbuild.2019.109353.
[34] Soliman A.M.A, Hassan H, Ahmed M, Ookawara S. A 3d model of the effect of using heat spreader on the performance of photovoltaic panel (PV). *Mathematics and Computers in Simulation* 2020; *167*: 78–91. DOI: 10.1016/j.matcom.2018.05.011.
[35] Said, M.A, Hassan, H. Effect of using nanoparticles on the performance of thermal energy storage of phase change material coupled with air-conditioning unit. *Energy Conversions and Management* 2018; *171*: 903–916. DOI: 10.1016/j.enconman.2018.06.051.
[36] Hassan, H. Heat transfer of Cu–water nanofluid in an enclosure with a heat sink and discrete heat source. *European Journal of Mechanics - B/Fluids* 2014; *45*: 72–83. DOI: 10.1016/j.euromechflu.2013.12.003.
[37] Bechiri, M, Mansouri K. Analytical study of heat generation effects on melting and solidification of nano-enhanced PCM inside a horizontal cylindrical enclosure. *Applied Thermal Engineering* 2016; *104*: 779–790. DOI: 10.1016/j.applthermaleng.2016.05.105.
[38] Vajjha, R.S, Das, D.K, Kulkarni, D.P. Development of new correlations for convective heat transfer and friction factor in turbulent regime for nanofluids. *International Journal of Heat and Mass Transfer* 2010; *53*: 4607–4618. DOI: 10.1016/J.IJHEATMASSTRANSFER.2010.06.032.